Appl. Phys. A 65, 525–534 (1997)

Applied Physics A Materials Science & Processing

Shape and stability of quantum dots

E. Pehlke*, N. Moll, A. Kley, M. Scheffler

Fritz-Haber-Institut der Max-Planck-Gesellschaft, Faradayweg 4–6, D-14195 Berlin-Dahlem, Germany
(E-mail: pehlke@physik.tu-muenchen.de)

Received: 21 March 1997/Accepted: 12 August 1997

Abstract. The formation of dislocation-free three-dimensional islands by heteroepitaxial growth of lattice mismatched materials is utilized to produce partially ordered arrays of quantum dots. The equilibrium shape of these islands results from the competition between surface and elastic energies. We have studied the system InAs/GaAs(001) in detail. InAs surface energies have been computed *ab initio* for several orientations, and the elastic energy of the islands has been calculated within a continuum theory. The resulting equilibrium islands are hills bounded by {110}, {111}, and $\{\bar{1}\bar{1}\bar{1}\}$ facets and a (001) surface on top. We compare to experiment and discuss the influence of growth kinetics on the shape.

PACS: 68.65.+g

Quantum dots have raised intense recent interest due to their peculiar electronic properties characteristic for a zero-dimensional system, which drastically differ from those of the bulk. In a sense they can be regarded as novel artificial materials. Technology can profit from these materials, using them, for example, to improve the performance of semiconductor devices (e.g., the quantum dot laser [1]) or even to construct new kinds of devices (e.g., the single electron transistor [2]). However, quantum dots are fascinating objects also for basic research, and the physics of these low-dimensional structures, such as quantum wires and quantum dots, represents a rapidly growing branch of semiconductor physics.

Quantum dots can be prepared by enclosing small three-dimensional islands of a low-bandgap semiconductor in a wide-bandgap semiconductor matrix. Provided the bands are appropriately aligned, the valence and conduction bands produce a confinement potential for the holes in the valence band and the electrons in the conduction band [3]. Thus the electronic density of states of the quantum dot consists of delta peaks as opposed to the continuous spectrum of the bulk. For this reasons such an island is sometimes referred to as a "super-atom", to emphasize this difference to a solid.

To act as a quantum dot, the size of the island has to lie within a certain range. The lower size limit follows from the requirement that the confinement potential has to have at least one bound state, i.e., the potential must not be too shallow. On the other hand, the islands should not exceed a certain size, else, when the energy-level spacing becomes too small, the desired quantum dot properties will be lost due to thermal smearing and evaporation of carriers from the dot. The size limitation depends on the material, e.g., for InAs quantum dots in GaAs Ledentsov [4] has given an estimate that the diameter of the islands should lie between 40 to 200 Å.

Such small structures are difficult to prepare by standard lithography techniques. However, one can exploit an effect that is well known in crystal growth but was for a long time considered only a nuisance for device fabrication, i.e., the roughening of a surface during heteroepitaxial growth [5, 6]. The aim of this work is to investigate the energetics of the strained coherent islands that form during Stranski-Krastanov growth of InAs on a GaAs(001) substrate, to derive the equilibrium shape of the islands and to discuss possible consequences concerning the stability of the islands and the basic physics governing the growth.

1 Stranski-Krastanov Growth

When a material is grown on a lattice-mismatched substrate, the elastic energy of a strained uniform film (UF) $E_{\mathrm{UF}} = c\varepsilon_0^2 V$ (c: elastic constant, ε_0: epitaxial strain, V: volume of the film) increases linearly with film thickness. Thus it becomes unstable beyond some critical thickness (see Fig. 1). Strain relaxation can be achieved by the introduction of dislocations and island formation. The energy of the dislocated islands (DI) is given by the sum of the excess surface energy $\gamma \Delta A$ (ΔA denotes the increase in surface area due to island formation) plus the island-substrate interface energy λA_0, which contains the energetical cost per area to create dislocations. Obviously, for sufficiently large film thickness it becomes energetically advantageous for the system to form

Invited paper presented at the DPG-Frühjahrstagung, Münster, Spring 1997.
**Present address*: Physik-Department T30, Technische Universität München, D-85747 Garching, Germany
Correspondence to: E. Pehlke, Technische Universität München

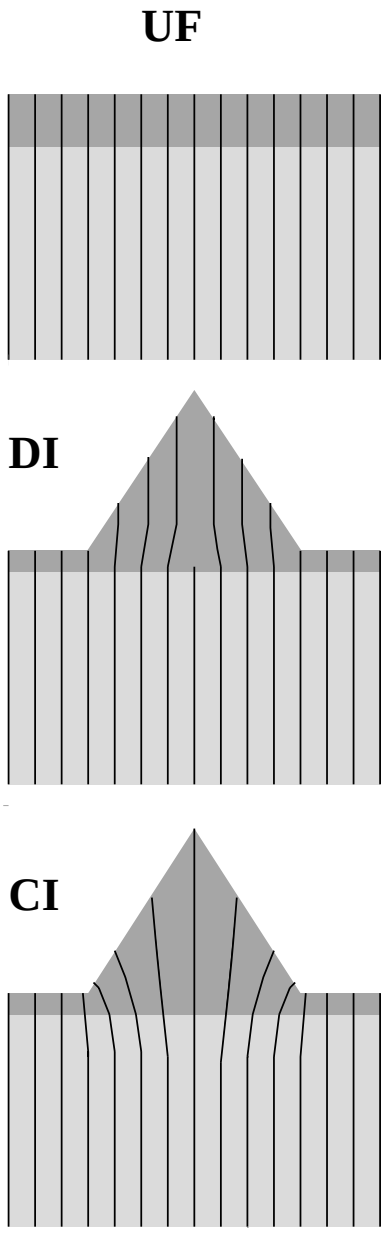

Fig. 1. Strain relaxation during Stranski-Krastanov growth (schematic). Light gray color denotes the substrate (GaAs), dark gray the lattice-mismatched overlayer (InAs). The lines symbolize lattice planes. It is assumed that surface and interface energies are such that the formation of a wetting layer is energetically preferred. Top (UF): uniform strained film, $E_{\mathrm{UF}} = c\epsilon_0^2 V$, Middle (DI): dislocated relaxed islands, $E_{\mathrm{DI}} = \gamma \Delta A + \lambda A_0$, Bottom (CI): coherent strained islands, $E_{\mathrm{CI}} = \gamma \Delta A + c\epsilon_0^2 V - E_{\mathrm{el}}$

such islands. However, there is another important and general mechanism of strain relaxation. For Ge grown on a Si(001) surface, Eaglesham and Cerullo [7] observed the formation of three-dimensional Ge islands that are dislocation-free. This change in surface morphology is driven by the gain in elastic relaxation energy E_{el} of the coherent islands (CI) as compared to the uniform film, which overcompensates the energetical cost $\gamma \Delta A$ due to the increase of surface area.

The energy gain due to formation of a single either coherent or dislocated island has been investigated by Vanderbilt and Wickham [8]. A schematic diagram showing the stability range of the three different configurations is shown in Fig. 2. Provided the interface energy for dislocated islands is sufficiently large, increasing the volume will result in a transition from a uniform film to coherent islands, which yield the energetically preferred morphology not only compared to the uniform film but also compared to dislocated islands. However, it is worthwhile noting that Fig. 2 is not a phase diagram [9]. When an ensemble of islands is considered, within the scope of the approach outlined above larger islands will grow on the expense of smaller ones, i.e., Ostwald ripening will take place.

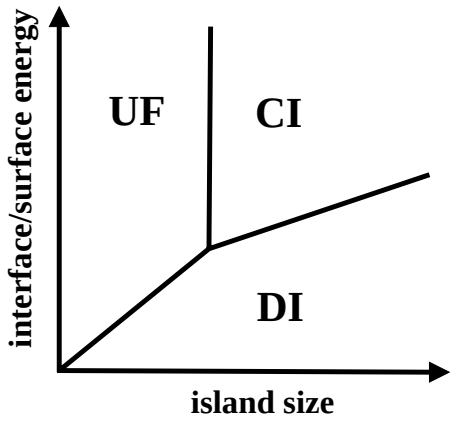

Fig. 2. Schematic diagram [8] showing the lowest energy configuration of a single heteroepitaxial island as a function of its volume and a material parameter, the ratio of interface to excess surface energy, which is a measure for the energy cost of dislocations at the substrate-island interface

The strain-induced self-assembly of small coherent islands has been applied successfully to produce ordered arrays of quantum dots [4]. A frequently studied material system is InAs/GaAs(001) [5, 10–20], with a large lattice mismatch of about 7%. A rather puzzling experimental observation has been the narrow width of the island size distribution [5, 11]. In fact this represents an important as well as desirable feature of quantum dot growth, because in general both in measurements and device applications the delta-function shaped electronic density of states of every single quantum dot will be smeared out by ensemble averaging over the size distribution. Thus it is important to understand the mechanism governing the size distribution; its narrowness appears to be incompatible with Ostwald ripening. Several mechanisms [21–24] have been suggested; however, even the question whether it is due to kinetics or energetics is still controversial.

In this article we will focus on the equilibrium shape of coherent three-dimensional InAs islands. Knowledge of the equilibrium shape as a function of volume is an essential prerequisite for deciding upon the true growth mechanism. Though kinetic effects will be important, three-dimensional islands close to equilibrium should be observable under appropriate experimental conditions: When the concentration of quantum dots is low, diffusion of atoms on a single island should be faster than material exchange between the islands. Thus shape equilibration should occur on a timescale faster than that of Ostwald ripening. Conversely, if already the experimentally observed shape deviates from the equilibrium shape, equilibrium thermodynamics will not be adequate to describe the island size distribution under the respective growth conditions.

It is not feasible, and also not necessary, to compute the total energy of an entire quantum dot within a single *ab initio* calculation. We have broken up the problem into two steps. First we compute InAs surface energies for several surface orientations by using density-functional theory. Then the elastic relaxation energy is calculated within continuum theory for the case of a low island concentration, applying a finite element approach. The total energy of the islands, including the elastic energy of the strain field in the substrate, is given by the sum of these two energy contributions. All the more delicate effects [22] like the strain-dependence of the surface energy are neglected for the purpose of predicting island shapes at fixed volume.

2 Surface energy

The stable surface reconstruction is the one with the lowest surface free energy. In case of two-component systems, like the surfaces of III–V compounds, the stoichiometry of the surface enters as an additional, chemical degree of freedom into the optimization. To compare surfaces of different stoichiometry, a chemical potential is introduced, which describes the energy it takes to extract an atom from the respective reservoir. The surface energy of area A as a function of chemical potential is

$$\gamma A = E_{\mathrm{surf}}(N_i) - \sum_i \mu_i N_i \,, \tag{1}$$

with μ_i denoting the free energy per particle in the reservoir of species i, and N_i the number of particles of species i. Chemical equilibrium requires that the sum of μ_{In} and μ_{As} equals μ_{InAs}, the energy per In-As pair in bulk InAs. Thus there is only one independent variable describing the chemical environment, which we take to be μ_{As}, and the surface energy is calculated from the total energy E_{tot} via

$$\gamma A = E_{\mathrm{tot}} - \mu_{\mathrm{InAs}} N_{\mathrm{In}} - \mu_{\mathrm{As}}(N_{\mathrm{As}} - N_{\mathrm{In}}) \,. \tag{2}$$

In the following we will discuss surface energies at zero temperature and pressure and neglect corrections from zero-point vibrations. We have carried out total-energy calculations within density-functional theory. Similar calculations for GaAs are described in [25]; details of the calculation can be found there. Hence only the main features of the computational procedure will be outlined below.

The local-density approximation is applied to the exchange-correlation energy-functional by using Perdew and Zunger's [26] parameterization of the correlation energy of the homogeneous electron gas [27]. Surfaces are approximated by periodically repeated slabs. For example, in case of the (111) orientation, we use a supercell with a (2×2) surface unit-cell and 10 atomic layers, the topmost 4 of which are fully relaxed. Atoms in the remaining layers are fixed at their bulk positions, and we use our theoretical lattice constant of 5.98 Å.

The simplest approach to calculate surface energies would be to take the same reconstruction on both sides of the slab. In that case the surface energy can directly be inferred from the total energy of the slab by subtracting the bulk energy [(2) gives the precise expression applicable also for nonstoichiometric slabs]. However, this approach does not work for arbitrary surface orientations. For example, (111)-slabs are built of a stack of In-As double layers, which are cation or anion terminated, respectively, on the opposite sides of the slab. Therefore the two surfaces of the slab are necessarily inequivalent. Chetty and Martin [28] solved this problem by introducing an energy density. Integrals of the energy density over suitably chosen subvolumes of the supercell, e.g., volumes bounded by bulk mirror planes, yield total energies that are well defined and can be interpreted as the energies of the top and bottom half of the slab. From these the surface energies of the top and bottom surface can be derived independently. We have implemented the energy density formalism into the `fhi93cp` plane-waves total-energy code [29]. Applying the energy density formalism, we have the freedom to choose different ways to terminate the slab on its bottom side. So we fix the atoms at their bulk positions and saturate all dangling bonds with hydrogen-like potentials [30] with atomic number $Z = 1.25$ for bonds to In atoms and $Z = 0.75$ for bonds to As atoms. Surfaces saturated in this way are semiconducting without any states in the bulk band-gap, and the interaction between the two surfaces of the slab is minimal.

The In and As atoms are described by norm-conserving *ab initio* pseudopotentials [31]. The *d*-potentials are chosen as the local potentials, and the nonlocal *s*- and *p*-potentials are cast into the Kleinman-Bylander [32] form. The wavefunctions are expanded into plane waves, with a kinetic energy cutoff of 10 Ry. The electron density is calculated using special $\boldsymbol{k}$-point sets [33] with a density in reciprocal space equivalent to 64 $\boldsymbol{k}$-points in the entire (100) (1×1) surface Brillouin zone.

InAs surfaces are expected to display surface reconstructions equivalent to those of GaAs. Therefore we have calculated the surface energy for the same structures as we already considered in [25] for GaAs. Atomic geometries and the corresponding surface energies as a function of chemical potential are displayed in Figs. 3–10.

For the (110) orientation in case of InAs always the relaxed (1×1) cleavage plane yields the lowest surface energy independent of the As chemical potential. The As-terminated (110) (1×1) surface, which for GaAs becomes stable under As-rich conditions [25], remains unstable. The relaxed cleavage surface displays the well-known outward rotation of the As-atom, investigated experimentally by Duke et al. [34] by using low-energy electron-diffraction.

For the (100) orientation our calculation yields the $\beta2(2 \times 4)$ reconstruction as the energetically preferred surface structure under As-rich conditions. Again, the most As-rich $c(4 \times 4)$ reconstruction, which becomes stable in As-rich environment in case of GaAs, does not become stable for InAs. Experimentally [35] the surface reconstruction has been reported to change from (2×4) to (4×2) as a function of As chemical potential; our calculated energy of the $\beta2(4 \times 2)$ reconstruction is somewhat too large to reproduce this transition.

Both for the (111) and the $(\bar{1}\bar{1}\bar{1})$ orientation our predicted equilibrium reconstructions are consistent with recent core-level and valence photoemission studies [36, 37]. While the As-trimer structure becomes the energetically preferred reconstruction of the GaAs (111) surface in As-rich environment, for InAs the stoichiometric In vacancy reconstruction is stable independent of the As chemical potential and the As-trimer structure remains always unstable. For the $(\bar{1}\bar{1}\bar{1})$ orien-

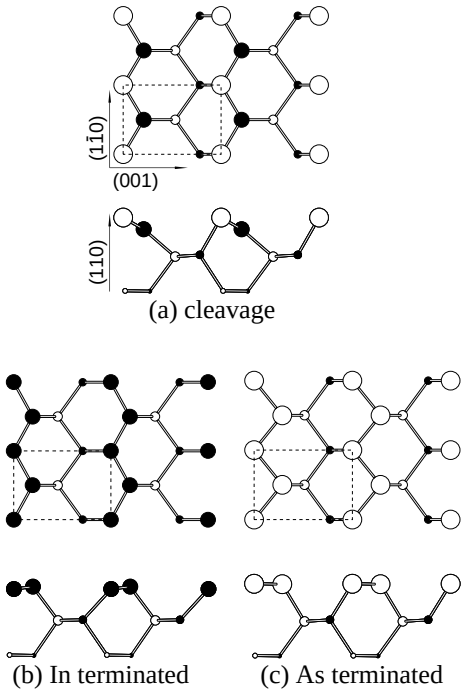

Fig. 3. Atomic structure models for the InAs(110) surface, top and side views. Open and filled circles denote As and In atoms, respectively

tation on the other hand both GaAs and InAs display equivalent surface reconstructions, with an As-trimer reconstruction being stable under As-rich conditions. On the GaAs $(\bar{1}\bar{1}\bar{1})$ surface a $(\sqrt{19}\times\sqrt{19})$ reconstruction characterized by two-layer hexagonal rings has been observed in Ga-rich environment by means of the scanning-tunneling microscope [38]. However, we have not yet carried out calculations for this reconstruction, which would be rather expensive due to the large unit cell.

Since epitaxial growth most often is performed under As-rich conditions, we will take the surface energies for surfaces in equilibrium with bulk arsenic (i.e., $\mu_{\mathrm{As}} = \mu_{\mathrm{As(bulk)}}$) when comparing island shapes etc. to experiment. For convenience, the surface energies are reproduced in Table 1. They are distinctly smaller than those of GaAs [25]. A significant part of

Table 1. The equilibrium surface reconstructions of InAs in equilibrium with bulk As and their surface energies

orientation	reconstruction	surface energy [meV/Å^2]
(110)	(1×1) relaxed cleavage plane	41
(100)	$\beta(2\times4)$	44
(111)	(2×2) In vacancy	42
$(\bar{1}\bar{1}\bar{1})$	(2×2) As trimer	36

the difference is simply due to the 7% larger lattice constant of InAs as compared to GaAs; in general for a given recon-

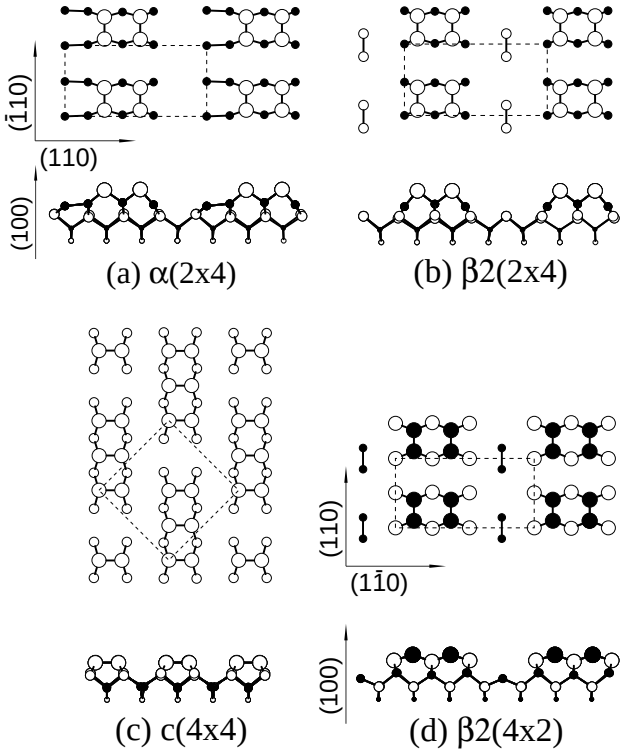

Fig. 5. Atomic structure models for the InAs(100) surface

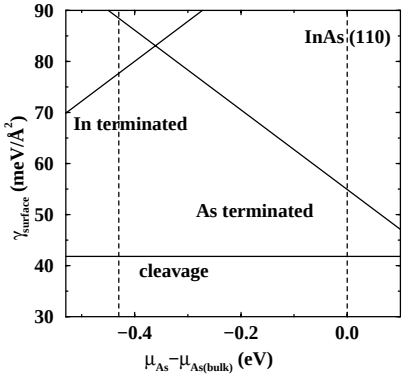

Fig. 4. Surface energy of various InAs(110) surface reconstructions as a function of the As chemical potential

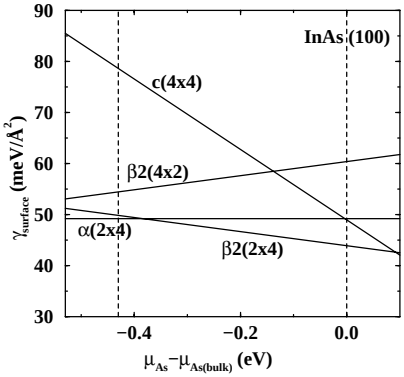

Fig. 6. Surface energy of various InAs(100) surface reconstructions as a function of the As chemical potential

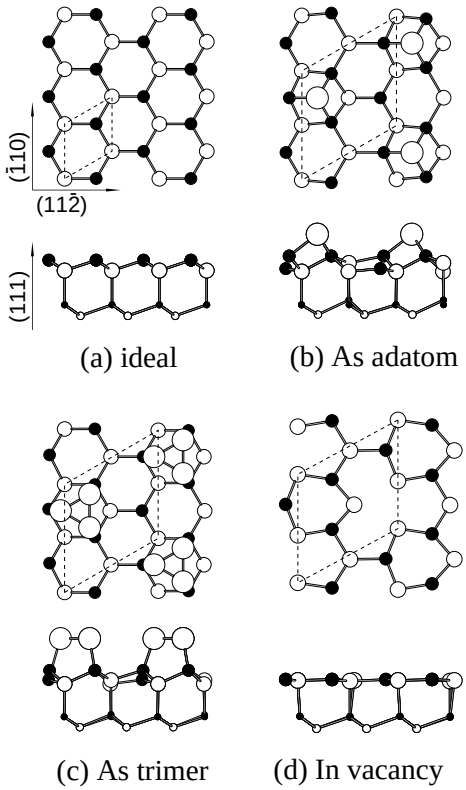

Fig. 7. Atomic structure models for the InAs(111) surface

struction, the energies per surface unit-cell differ less between the two materials than the energies per surface area.

Let us now consider an unstrained free-standing InAs crystal that is perfectly equilibrated. It will adopt a certain shape, which minimizes the total surface energy at fixed volume. In the thermodynamic limit of infinitely large volume this is called the equilibrium crystal shape (ECS). We have calculated the ECS of InAs in As-rich environment, applying the Wulff construction to the data in Table 1; the result is displayed in Fig. 11. Since only the surface energies for the {110}, {100}, {111}, and $\{\bar{1}\bar{1}\bar{1}\}$ orientations enter our Wulff construction, we cannot exclude that additional orienta-

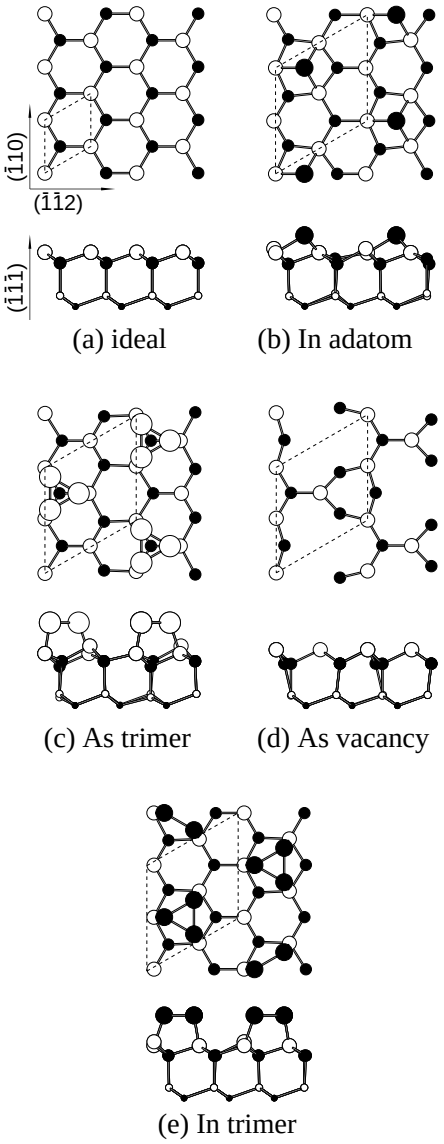

Fig. 9. Atomic structure models for the InAs($\bar{1}\bar{1}\bar{1}$) surface

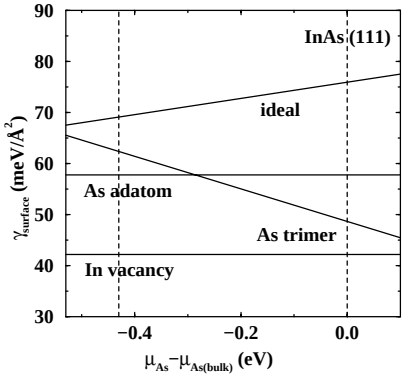

Fig. 8. Surface energy of various InAs(111) surface reconstructions as a function of the As chemical potential

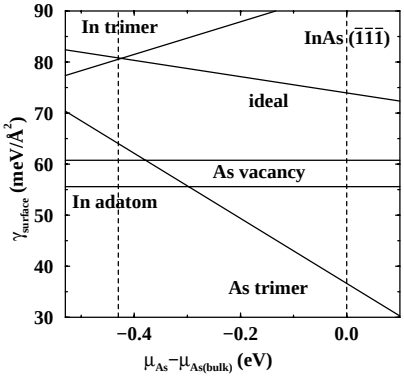

Fig. 10. Surface energy of various InAs($\bar{1}\bar{1}\bar{1}$) surface reconstructions as a function of the As chemical potential

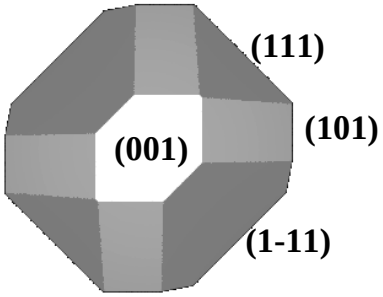

Fig. 11. Equilibrium shape of InAs in As-rich environment. Surfaces are labelled by their Miller indices

tions might appear on the ECS, however the low Miller-index orientations are expected to be the most prominent ones. In fact we find that all four surface orientations {110}, {100}, {111}, and $\{\bar{1}\bar{1}\bar{1}\}$ co-exist on the ECS, i.e., these surfaces are thermodynamically stable with respect to faceting. This is in agreement with the observed shape of large, and thus presumably fully relaxed, InAs islands grown on a GaAs substrate by metal-organic vapour-phase epitaxy by Steimetz et al. [39].

3 Elastic relaxation energy

In addition to the surface energies, the equilibrium shape of the coherent strained islands is controlled by the elastic relaxation energy. We have calculated the elastic energy within a continuum approach. The experimental second- and third-order elastic moduli of GaAs [40] are used to describe the elastic properties of both the substrate and the island. This approximation does not affect our conclusions, as has been shown by additional calculations by using the linear elastic constants of GaAs and InAs. A finite element approach is applied to solve the nonlinear elasticity problem. Both the island and a sufficiently thick slab representing the substrate are divided into small irregularly shaped tetrahedra. The displacement field $\boldsymbol{u}(\boldsymbol{r})$ is tabulated on the vertices of this partitioning. Within each tetrahedron the linear interpolation uniquely determined by the values of $\boldsymbol{u}$ at the four corners of the tetrahedron is taken for $\boldsymbol{u}(\boldsymbol{r})$. Therewith the strain tensor $\varepsilon(\boldsymbol{r})$ becomes piecewise constant. The total elastic energy is calculated by summing the elastic energy density within each tetrahedron, which is a function of local strain, times the volume of the tetrahedron over all tetrahedra. This expression is iteratively minimized with respect to the displacement field. This procedure is repeated for finer and finer partitioning of the volume and the results are finally extrapolated to fineness equal to zero.

In searching for the equilibrium island shape, many different geometries have to be considered. However, for some geometries we can avoid repeating the full finite-element calculation and instead use a simple analytic approach that gives a sufficiently accurate approximate answer (see also [41]). Our approach is based on the scaling law of elastic energy with volume and the observation, that the tops of pyramidal islands with {101} or {111} and $\{\bar{1}\bar{1}\bar{1}\}$ faces are almost completely relaxed. Let E_{pyr} denote the elastic energy of a strained pyramid-shaped epitaxial island with volume V. We create a truncated pyramid with energy E' and volume V' by slicing off the top of the pyramid with a (001) plane. From the variational property of the elastic energy as a functional of $\boldsymbol{u}(\boldsymbol{r})$, we get an estimate for E':

$$E' \leq E_{\mathrm{pyr}} - \int\limits_{V \setminus V'} f\big(\varepsilon(\boldsymbol{r})\big)\, \mathrm{d}^3\boldsymbol{r}\,, \tag{3}$$

the integral representing the elastic energy contained in that part of the pyramid that has been sliced off. Finally we make use of the scaling law $E_{\mathrm{elast}} \sim V$ to transform E' from V' back to the original volume V and in this way get the energy E_{mesa} of a truncated pyramid with volume V:

$$E_{\mathrm{mesa}} \leq V/V' \left(E_{\mathrm{pyr}} - \int\limits_{V \setminus V'} f\big(\varepsilon(\boldsymbol{r})\big)\, \mathrm{d}^3\boldsymbol{r} \right). \tag{4}$$

In the following we are going to even neglect the contribution from the integral in (4). This simple approximation yields satisfying results as can be judged from Fig. 12 in the following

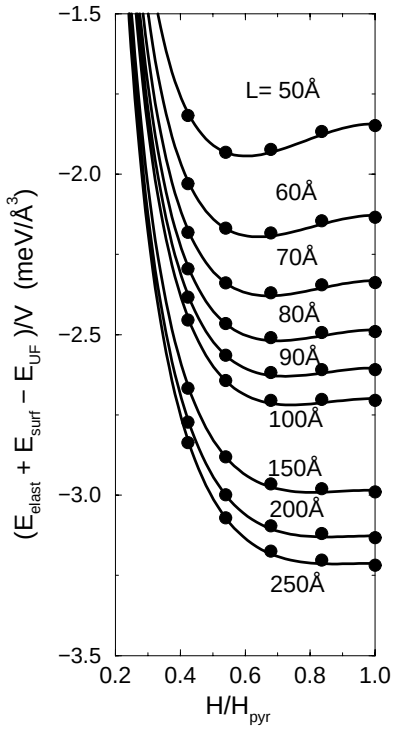

Fig. 12. Energy gain due to formation of coherent islands in comparison to a strained uniform film. The elastic energy E_{elast} plus the surface energy E_{surf} minus the energy of the corresponding uniform strained film E_{UF} is plotted vs. the height H of the truncated pyramid, normalized to the height H_{pyr} of a pyramid with the same volume. The truncated pyramids are bounded by four {110} facets and one (001) facet. The curves are parameterized by the width L of the pyramid, which just represents a simple measure for the volume. The filled circles denote computed values, while the lines represent the analytic approximation discussed in Sect. 3 where the strain energy in the almost relaxed top of the pyramid is neglected

Section. The full lines, based on the approximation $V/V' E_{\rm pyr}$ for the elastic energy $E_{\rm mesa}$, pass through the data points computed with the finite-element code.

4 Equilibrium island shape

The equilibrium shape of a strained coherent epitaxial island is derived by minimizing its total energy with respect to its shape. The total energy is approximated by the sum of the elastic energy and the surface energies of all facets forming the island, less the surface energy of that portion of the (001) plane that is covered by the island. Owing to the different scaling properties of the elastic and the surface energy, the optimum island shape depends on volume.

To illustrate the main physical mechanism of how strain effects change the morphology of islands, we first restrict ourselves to a very small portion of configuration space. We consider only a square based pyramid with four {101} faces and the related truncated pyramids terminated by an additional (001) plane on top. The size of each mesa-shaped island is adjusted in such a way that its volume stays equal to the volume of the original pyramid. When a truncated pyramid is created in this way, the elastic energy increases in comparison to the elastic energy of the original pyramid because material from the top of the pyramid, where it is almost completely relaxed, is deposited into the remaining mesa, where it is under considerable strain. On the other hand, given the InAs surface energies in Table 1, the total surface energy decreases. The optimum configuration results from the competition between these two energy contributions. However, the variation with island size differs for these two contributions. While the elastic energy scales linearly with volume V, the total surface energy is proportional to the surface area, i.e., it scales with $V^{2/3}$. Therefore the optimum shape becomes a function of volume, with the surface energy being more important at small volume and the elastic energy dominating at large volume. This explains the results displayed in Fig. 12. For small island volume, the total energy gain due to island formation adopts its optimum for some mesa-shaped island. When the volume is increased, the strain effects gain more influence. Accordingly the minimum of the total energy curves becomes less pronounced and shifts towards the pyramidal geometry. One should keep in mind, however, that, from a practical point of view, the range of island size for which above scaling arguments are applicable is limited. For $V \to 0$, atomistic effects and two-dimensional islands (for which the dependence of elastic energy on size is perfectly different) will become important, while for large volumes the preferred relaxation mechanism will change and dislocations will be generated at the island-substrate interface.

To derive the equilibrium island shape, we now have to account for the whole variety of possible island configurations. However, it is sensible to first restrict this search to those surface orientations that appear on the ECS (Fig. 11). Surfaces with a smaller slope than the (101) plane that do not exist on the ECS could facet into the thermodynamically stable orientations {101}, {111}, $\{\bar{1}\bar{1}\bar{1}\}$, and (001). In general, bulk strain effects should further aid this process because they tend to favor islands with steeper faces, while there is no *a priori* estimate for the contribution from surface stress. We have calculated the elastic and surface energies only for various arbitrarily shaped InAs islands bounded by {101}, {111}, and $\{\bar{1}\bar{1}\bar{1}\}$ facets. The results are displayed by filled symbols in Fig. 13. The elastic energies of the related (001)-truncated "mesa-shaped" islands have been derived from the simple analytic approximation introduced in Sect. 3, the corresponding results are marked by open circles in Fig. 13.

The optimum island shape at a given volume is determined by that point where the line of constant total energy touches the manifold of island energies from below. Even when the volume is changed we can nevertheless still read the optimum shape from the same graph. From the scaling relations, we know that the ordinate does not change, while the abscissa has to be rescaled according to $E_{\rm surf}/V \sim V^{-1/3}$. Therefore only the slope of the total energy line decreases when the volume increases, and hence the whole evolution of equilibrium island shape with volume can be extracted from Fig. 13.

The equilibrium islands are hills bounded by {101}, {111}, and $\{\bar{1}\bar{1}\bar{1}\}$ faces and a (001) surface on the top (see Fig. 14). As explained above, owing to the different scaling properties of elastic and surface energy larger islands are steeper than the smaller ones. This can be recognized in Fig. 14 by comparing the relative sizes of the (101) and (111) or $(1\bar{1}1)$ faces of the two islands. At larger volume, the steeper (111) and $(1\bar{1}1)$ faces become more prominent. Our calculated island shape is similar to the shape of InP islands on GaInP observed by Georgsson *et al.* [42]. However, the surface energies of InP will differ from those of InAs, making this comparison diffi-

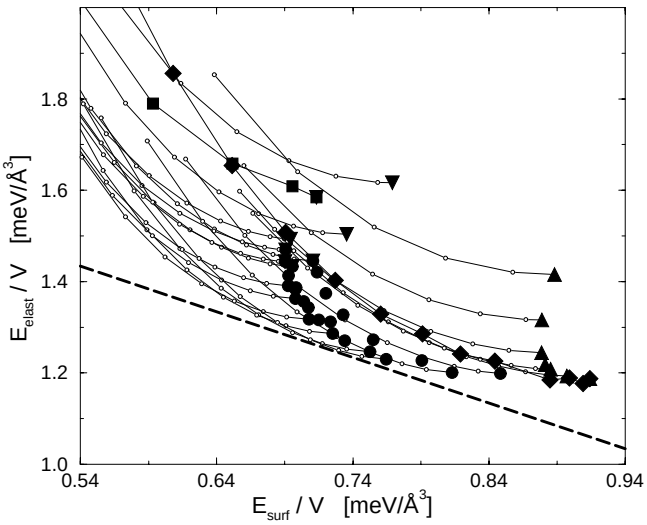

Fig. 13. Elastic energy per volume $E_{\rm elast}/V$ vs. surface energy per volume $E_{\rm surf}/V$ for InAs islands with volume $V = 2.88 \times 10^5$ Å^3. Squares, square based pyramid with four {101} faces and (001)-truncated {101}-pyramids. Diamonds, square based pyramids with two {111} and two $\{\bar{1}\bar{1}\bar{1}\}$ faces and (001)-truncated pyramids. Triangles up, "huts" with two {111} and two $\{\bar{1}\bar{1}\bar{1}\}$ faces. Triangles down, square based {101} pyramids with $\{\bar{1}\bar{1}\bar{1}\}$-truncated edges. Dots, islands with four {101}, two {111}, and two $\{\bar{1}\bar{1}\bar{1}\}$ faces. Filled symbols denote numerical results, while open circles have been calculated using the simple analytical approximation for (001)-truncated "mesa-shaped" islands described in Sect. 3, assuming that the elastic energy does not change when the almost fully relaxed top of the island is cut off. Full lines connect islands that are created in this way, varying the height of the (001) surface plane. The dashed line is the curve of constant total energy $E_{\rm elast} + E_{\rm surf}$ that selects the equilibrium shape (for the particular volume $V = 2.88 \times 10^5$ Å^3)

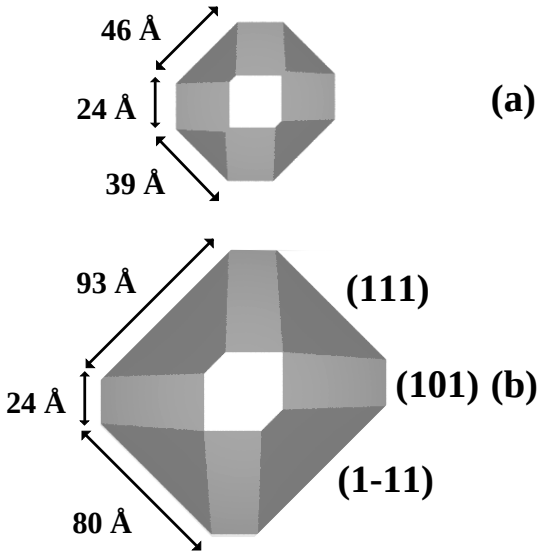

Fig. 14a,b. The equilibrium shape of strained coherent InAs islands at two different volumes, **a** $V = 8 \times 10^4$ Å^3, **b** $V = 36 \times 10^4$ Å^3

cult as long as no density-functional results are available for this material. Various shapes have been reported for InAs islands grown on GaAs(001). Moison et al. [11] have observed rather flat islands having {410} facets. Nabetani et al. [14] report {113}A-facets. Leonard et al. [12] describe the shapes as planoconvex lenses with a radius to height aspect ratio of about 2. The InAs islands grown on GaAs(001) by Ruvimov *et al.* [16, 43] are {101}-bounded pyramids. These shapes differ from the equilibrium shape predicted theoretically. In the following Sect., we will consider effects that can cause a deviation of the experimentally observed shape from the equilibrium island shape discussed above.

Finally we note that due to the continuous change of the optimum island shape with the size, both the surface energy and elastic energy of the equilibrium islands do not follow the simple scaling laws $E_{\text{surf}} \sim V^{2/3}$ and $E_{\text{elast}} \sim V$ any more. Instead, the total energy of the equilibrium islands can be derived from a Legendre transform of the low-energy envelope of the data in Fig. 13. Of course our approach still leads to Ostwald ripening by means of its construction. To allow for the possibility of an equilibrium island size further interactions would have to be considered [22].

5 Discussion

Next we consider additional possible mechanisms that might affect the shape of the coherent islands.

The equilibrium crystal shape displayed in Fig. 11 refers to a crystal in As-rich environment. The As chemical potential has been fixed at $\mu_{\text{As(bulk)}}$, because this is expected to reasonably reflect typical experimental conditions during molecular beam epitaxial growth. However, if μ_{As} is varied, the InAs surface energy changes for the $(\bar{1}\bar{1}\bar{1})$ orientation, and also slightly for the (001) orientation; therefore the crystal will adopt a different equilibrium shape. The surface energy of the (110) orientation imposes an upper limit of $\sim 50\,\text{meV/Å}^2$ on the energy of a stable $(\bar{1}\bar{1}\bar{1})$. From Fig. 10 we have to conclude that the $(\bar{1}\bar{1}\bar{1})$ surface will thus become thermodynamically unstable for $\mu_{\text{As}} < \mu_{\text{As(bulk)}} - 0.2$ eV, as far as no other reconstruction, like the $(\sqrt{19} \times \sqrt{19})$, more stable than the In adatom structure comes into play. On the other hand, the energies of both the InAs (110) and (111) surface do not depend on the As chemical potential. Therefore the {111} faces will exist on the ECS independent of μ_{As}.

The variation of the surface energy due to the strain at the surface has been neglected so far. Here we will give a very rough estimate for this effect, only considering the linear term $\varepsilon_{ij}\sigma_{ij}$ but no higher-order terms [22]. We have calculated the stress of the GaAs (110) (1×1) surface to be tensile and equal to $20\,\text{meV/Å}^2$ parallel to [001] and $57\,\text{meV/Å}^2$ parallel to $[1\bar{1}0]$. Furthermore we assume that about 30% of the total {110} surface area is strained (we simply take the epitaxial strain though the true surface strain tensor will be anisotropic) while the rest is assumed to be completely relaxed. Then the decrease of the average (110) surface energy due to strain becomes $\Delta\gamma = -1.6\,\text{meV/Å}^2$. However, in order to drive the (111) surface (which has a surface energy equal to $41.5\,\text{meV/Å}^2$) unstable with respect to faceting into {110} surfaces, the (110) surface energy would have to be lowered by about $7.3\,\text{meV/Å}^2$, which is still larger by a factor of four than the strain effect estimated above. Thus, though the surface stress is rather important and should be included in a more refined version of the theory of the equilibrium island shape, it does not appear to be sufficient to completely suppress the {111} surfaces on the theoretical shapes.

Finite size effects with respect to the surface energies might also play a role for the shape of the equilibrium islands. Facets are small, containing only of the order of 100 atoms for a typical quantum dot, and this may impede the formation of reconstructions with large surface unit-cells on small islands. Furthermore, a considerable part of the atoms in a facet form edge-atoms. Edge energies are not included in our calculation of the equilibrium shape, mainly because no reliable numbers are available, but also because they scale with island volume only like $V^{1/3}$. The general trend will be to reduce energy by reducing the length of the edges. For example, if the {101}/{111} edge would have a sufficiently high energy per length, total energy could be lowered by shrinking the {111} facets. The {101} facets are preferred by this mechanism for a geometrical reason: As the (111) plane is steeper than the (101) plane, peaked islands [i.e., those without a (001) facet on top] in general display {101} facets close to the top and {111} or $\{1\bar{1}1\}$ facets at their sides. These side facets will shrink when edges are shortened. This effect loses importance for larger islands; in particular both the {111} and the $\{\bar{1}\bar{1}\bar{1}\}$ facets are in fact clearly visible on the large, dislocated InAs islands observed in experiment [39].

As Jesson et al. [23] have pointed out for the Ge/Si system, kinetic effects originating from the strain of the island can result in self-limited growth and thus lead to a narrow island size distribution. Moreover kinetic effects can as well change the shape of the islands. As depicted in Fig. 15, there is a belt of highly strained material close to the foot of the island. If we assume that an additional layer preferentially nucleates at the edge between the island and the substrate surface as outlined in Fig. 16, the deposited material at the bottom of the island will be highly strained. Thus the elastic energy per volume is not constant; instead it fluctuates ac-

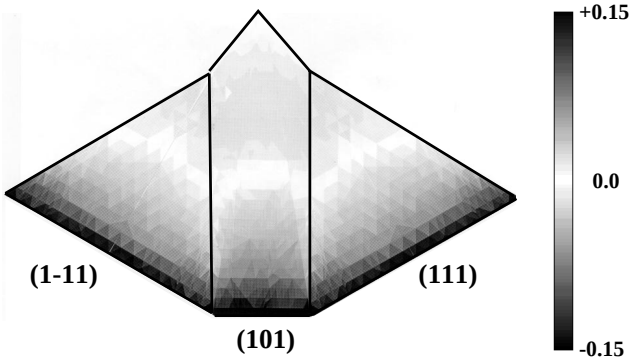

Fig. 15. Surface strain. The strain tensor has been calculated for a typical epitaxial island with {101}, {111}, and $\{1\bar{1}1\}$ faces [but for simplicity without the (001)-plateau on top], all with the same distance from the origin. The strain at the surface is defined by the appropriate two-dimensional trace of the strain tensor. Figure 15 shows a top view of the pentagonal (101) face and of the two adjacent triangular $(1\bar{1}1)$ and (111) faces, which have both been folded forward into the plane of the drawing. The local strain of the $(1\bar{1}1)$, (101), and (111) surfaces has been converted into a grayshade and plotted on the surface. The dark region at the bottom is due to the large local compression of the InAs close to the interface with the GaAs substrate

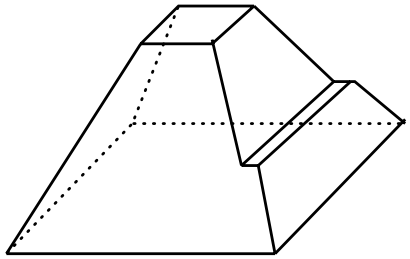

Fig. 16. Island having the shape of a truncated pyramid. An additional layer of material is growing on one of its faces. It is assumed that the layer nucleates at the edge between the island and substrate surface. In that case the newly deposited material is under large strain because it is located close to the bottom of the island

cording to the layer by layer growth. The kinetic barrier that arises is proportional to the volume of the deposited layer, thereby hindering the growth of large islands and narrowing the island size distribution in comparison to what would be expected for simple Ostwald ripening. Furthermore, for a given island the kinetic barrier will be small for a small facet and large for a large side facet of the island. Provided the growth of the facets proceeds layer-by-layer in the simple way depicted in Fig. 16, this implies that material will preferentially be deposited on the smaller facet, which thus will grow faster and, finally, will vanish. This means that, if the {111} and $\{\bar{1}\bar{1}\bar{1}\}$ facets are already sort of small (for example, due to the additional energetical effects discussed above and not accounted for in Fig. 14), the strain-induced barrier might finally make this facet kinetically unstable.

6 Summary and Conclusion

We have calculated the equilibrium shape of strained coherent InAs islands grown on a GaAs substrate by minimizing their total energy. The total energy is approximated by the sum of the surface energies and the elastic energy.

InAs surface energies have been computed *ab initio* for the {110}, {100}, {111}, and $\{\bar{1}\bar{1}\bar{1}\}$ orientations. The equilibrium crystal shape is derived from these results by means of the Wulff construction. In As-rich environment all four surface orientations co-exist on the ECS, which implies that they are stable with respect to faceting. This is consistent with the experimentally observed shape of large, presumably relaxed InAs islands [39].

The elastic relaxation energy is calculated within a continuum model by using a finite-element approach. The equilibrium islands are hills bounded by {110}, {111}, and $\{\bar{1}\bar{1}\bar{1}\}$ facets and a (001) surface on top. They are similar to the ECS in that they display all four different types of facets. The equilibrium island shape depends on size, i.e., large islands are steeper.

While similar island shapes have been observed in the material system InP/GaInP [42], our theoretical shape differs from the {101}-bounded InAs pyramids grown by Ruvimov et al. [16, 43] and the flatter island shapes observed by other authors. We have discussed several energy corrections that go beyond the simple approach outlined above and might result in somewhat more prominent {101} facets; in particular, the larger (2×2) surface reconstructions might be disadvantageous for very small facets. The residual difference between the equilibrium island shape and the kinetic growth shape is regarded as an indication for a kinetic barrier, which is induced by the large strain close to the bottom of the island. As suggested by Jesson et al. [23] and Chen and Washburn [44], such a barrier would also explain the narrowing of the island size distribution.

Acknowledgements. We thank E. Steimetz for helpful discussions and a copy of [39] prior to publication. This work was supported in part by the Sfb 296 of the Deutsche Forschungsgemeinschaft.

References

1. N. Kirstaedter, N.N. Ledentsov, M. Grundmann, D. Bimberg, V.M. Ustinov, S.S. Ruvimov, M.V. Maximov, P.S. Kop'ev, Zh.I. Alferov, U. Richter, P. Werner, U. Gösele, J. Heydenreich: Electron. Lett. **30**, 1416 (1994)
2. M.A. Kastner: In *Proceedings of the 23rd International Conference on the Physics of Semiconductors*, ed. by M. Scheffler, R. Zimmermann (World Scientific, Singapore 1996) p. 27
3. M. Grundmann, O. Stier, D. Bimberg: Phys. Rev. B **52**, 11969 (1995)
4. N.N. Ledentsov: In *Proceedings of the 23rd International Conference on the Physics of Semiconductors*, ed. by M. Scheffler, R. Zimmermann (World Scientific, Singapore 1996) p. 19
5. D. Leonard, M. Krishnamurthy, C.M. Reaves, S.P. Denbaars, P.M. Petroff: Appl. Phys. Lett. **63**, 3203 (1993)
6. W. Seifert, N. Carlsson, M. Miller, M.E. Pistol, L. Samuelson, L.R. Wallenberg: Progr. Cryst. Growth Charact. **33**, 423 (1996)
7. D.J. Eaglesham, M. Cerullo: Phys. Rev. Lett. **64**, 1943 (1990)
8. D. Vanderbilt, L.K. Wickham: In *Evolution of Thin-Film and Surface Microstructure, MRS Symposia Proceedings No. 202*, ed. by C.V. Thompson, J.Y. Tsao, D.J. Srolovitz (Material Research Society, Pittsburgh 1991) p. 555
9. B.G. Orr, D. Kessler, C.W. Snyder, L. Sander: Europhys. Lett. **19**, 33 (1992)
10. C.W. Snyder, B.G. Orr, D. Kessler, L.M. Sander: Phys. Rev. Lett. **66**, 3032 (1991)
11. J.M. Moison, F. Houzay, F. Barthe, L. Leprince, E. André, O. Vatel: Appl. Phys. Lett. **64**, 196 (1994)
12. D. Leonard, K. Pond, P.M. Petroff: Phys. Rev. B **50**, 11687 (1994)
13. P. Chen, Q. Xie, A. Madhukar, L. Chen, A. Konkar: J. Vac. Sci. Technol. B **12**, 2568 (1994)

14. Y. Nabetani, T. Ishikawa, S. Noda, A. Sasaki: J. Appl. Phys. **76**, 347 (1994)
15. X.W. Lin, Z. Liliental-Weber, J. Washburn, E.R. Weber, A. Sasaki, A. Wakahara, Y. Nabetani: J. Vac. Sci. Technol. B **12**, 2562 (1994)
16. S. Ruvimov, P. Werner, K. Scheerschmidt, U. Gösele, J. Heydenreich, U. Richter, N.N. Ledentsov, M. Grundmann, D. Bimberg, V.M. Ustinov, A.Yu. Egorov, P.S. Kop'ev, Zh.I. Alferov: Phys. Rev. B **51**, 14766 (1995)
17. V. Bressler-Hill, S. Varma, A. Lorke, B.Z. Nosho, P.M. Petroff, W.H. Weinberg: Phys. Rev. Lett. **74**, 3209 (1995)
18. M. Grundmann, J. Christen, N.N. Ledentsov, J. Böhrer, D. Bimberg, S.S. Ruvimov, P. Werner, U. Richter, U. Gösele, J. Heydenreich, V.M. Ustinov, A.Yu. Egorov, A.E. Zhukov, P.S. Kop'ev, Zh.I. Alferov: Phys. Rev. Lett. **74**, 4043 (1995)
19. H. Yamaguchi, M.R. Fahy, B.A. Joyce: Appl. Phys. Lett. **69**, 776 (1996)
20. P.M. Petroff, G. Medeiros-Ribeiro: MRS Bulletin **21**, 50 (1996)
21. C. Priester, M. Lannoo: Phys. Rev. Lett. **75**, 93 (1995)
22. V.A. Shchukin, N.N. Ledentsov, P.S. Kop'ev, D. Bimberg: Phys. Rev. Lett. **75**, 2968 (1995)
23. D.E. Jesson, K.M. Chen, S.J. Pennycook: MRS Bulletin **21**, 31 (1996)
24. C. Duport, C. Priester, J. Villain: to be published
25. N. Moll, A. Kley, E. Pehlke, M. Scheffler: Phys. Rev. B **54**, 8844 (1996)
26. J.P. Perdew, A. Zunger: Phys. Rev. B **23**, 5048 (1981)
27. D.M. Ceperley, B.J. Alder: Phys. Rev. Lett. **45**, 566 (1980)
28. N. Chetty, R.M. Martin: Phys. Rev. B **45**, 6074 (1992)
29. R. Stumpf, M. Scheffler: Comput. Phys. Commun. **79**, 447 (1994)
30. K. Shiraishi: J. Phys. Soc. Jap. **59**, 3455 (1990)
31. G.B. Bachelet, D.R. Hamann, M. Schlüter: Phys. Rev. B **26**, 4199 (1982)
32. L. Kleinman, D.M. Bylander: Phys. Rev. Lett. **48**, 1425 (1982)
33. H.J. Monkhorst, J.D. Pack: Phys. Rev. B **13**, 5188 (1976)
34. C.B. Duke, A. Paton, A. Kahn, C.R. Bonapace: Phys. Rev. B **27**, 6189 (1983)
35. H. Yamaguchi, Y. Horikoshi: Phys. Rev. B **51**, 9836 (1995)
36. L.Ö. Olsson, L. Ilver, J. Kanski, P.O. Nilsson, C.B.M. Andersson, U.O. Karlsson, M.C. Hakansson: Phys. Rev. B **53**, 4734 (1996)
37. C.B.M. Andersson, U.O. Karlsson, M.C. Hakansson, L.Ö. Olsson, L. Ilver, J. Kanski, P.O. Nilsson: Surf. Sci. **347**, 199 (1996)
38. D.K. Biegelsen, R.D. Bringans, J.E. Northrup, L.E. Swartz: Phys. Rev. Lett. **65**, 452 (1990)
39. E. Steimetz, F. Schienle, J.T. Zettler, W. Richter: J. Cryst. Growth **170**, 208 (1997)
40. *Data in Science and Technology, Semiconductors, Group IV Elements and III-V Compounds*, ed. by O. Madelung (Springer, Berlin 1991)
41. S. Christiansen, M. Albrecht, H.P. Strunk, P.O. Hansson, E. Bauser: Appl. Phys. Lett. **66**, 574 (1995)
42. K. Georgsson, N. Carlsson, L. Samuelson, W. Seifert, L.R. Wallenberg: Appl. Phys. Lett. **67**, 2981 (1995)
43. N.N. Ledentsov, V.A. Shchukin, M. Grundmann, N. Kirstadter, J. Böhrer, O. Schmidt, D. Bimberg, V.M. Ustinov, A.Yu. Egorov, A.E. Zhukov, P.S. Kop'ev, S.V. Zaitsev, N.Yu. Gordeev, Zh.I. Alferov, A.I. Borovkov, A.O. Kosogov, S.S. Ruvimov, P. Werner, U. Gösele, J. Heydenreich: Phys. Rev. B **54**, 8743 (1996)
44. Y. Chen, J. Washburn: Phys. Rev. Lett. **77**, 4046 (1996)